nature chemical biology

ARTICLES

https://doi.org/10.1038/s41589-018-0038-z

The cyanobacterial ornithine–ammonia cycle involves an arginine dihydrolase

Hao Zhang[1,2], Yujie Liu[1,2], Xiaoqun Nie[1,2], Lixia Liu[1], Qiang Hua[3], Guo-Ping Zhao[1,4,5] and Chen Yang[1*]

Living organisms have evolved mechanisms for adjusting their metabolism to adapt to environmental nutrient availability. Terrestrial animals utilize the ornithine–urea cycle to dispose of excess nitrogen derived from dietary protein. Here, we identified an active ornithine–ammonia cycle (OAC) in cyanobacteria through an approach combining dynamic ^{15}N and ^{13}C tracers, metabolomics, and mathematical modeling. The pathway starts with carbamoyl phosphate synthesis by the bacterial- and plant-type glutamine-dependent enzyme and ends with conversion of arginine to ornithine and ammonia by a novel arginine dihydrolase. An arginine dihydrolase–deficient mutant showed disruption of OAC and severely impaired cell growth when nitrogen availability oscillated. We demonstrated that the OAC allows for rapid remobilization of nitrogen reserves under starvation and a high rate of nitrogen assimilation and storage after the nutrient becomes available. Thus, the OAC serves as a conduit in the nitrogen storage-and-remobilization machinery in cyanobacteria and enables cellular adaptation to nitrogen fluctuations.

The ornithine–urea cycle (OUC) driven by carbamoyl phosphate synthase (CPS) type I is an essential metabolic pathway for the detoxification of ammonium and disposal of excess nitrogen in terrestrial animals, because a large quantity of ammonium is produced in the catabolism of protein from their diets[1,2]. Among the five OUC enzymes, four catalyze arginine-biosynthesis reactions, and the fifth, arginase, converts arginine to ornithine and urea. The OUC is also present in marine elasmobranchs and diatoms[2,3]. However, bacteria and plants are generally thought to lack a functioning OUC because they possess glutamine-dependent CPS type II instead of the ammonia-dependent CPS type I enzyme. The pathway is thus considered to constitute a waste of energy and assimilated nitrogen in these organisms[4,5].

Cyanobacteria are a large group of prokaryotes that, like plants, can perform oxygenic photosynthesis. They are found in diverse ecological habitats and substantially contribute to global carbon and nitrogen cycling[6,7]. A large amount of nitrogen is required for cyanobacterial cell growth. Among the various types of nitrogen sources that they can utilize, nitrate is the most abundant form of combined nitrogen available to cyanobacteria. Nitrate is converted to ammonia and is subsequently assimilated through the glutamine synthetase (GS)–glutamate synthase (GOGAT) cycle[8]. Nitrogen starvation induces chlorosis in many cyanobacteria, which is characterized by degradation of the light-harvesting antennae (phycobilisomes) and by a color change from blue-green to yellow-green[9]. In addition to phycobilisomes, another nitrogen reserve in most cyanobacteria appears to be cyanophycin, a nonribosomally synthesized peptide composed of arginine and aspartate[10]. Many strains of cyanobacteria are able to fix dinitrogen (N_2) in the absence of combined nitrogen. Cyanophycin has been shown to act as a dynamic reservoir for newly fixed nitrogen in diazotrophic cyanobacteria[11–13]. Although several studies have reported steady-state abundance of transcripts, proteins, and metabolites in cyanobacteria grown under nitrogen depletion-and-repletion conditions[14–16], how cyanobacteria dynamically modulate their metabolic network to give rise to rapid and adaptive responses to environmental nitrogen fluctuations remains largely to be elucidated. Understanding of how photosynthetic organisms adjust their metabolism to enable adaptation to changes in the nitrogen supply may aid in improving nitrogen-use efficiency in plants[17–19].

Recent progress in isotope tracer techniques and mass spectrometry (MS)-based metabolomics has allowed for quantitative monitoring of the dynamic responses of cellular metabolism to environmental perturbations[20–24]. In this study, we combined dynamic ^{15}N and ^{13}C tracer experiments, MS-based metabolomics analysis, and mathematical modeling to determine the mechanisms used by cyanobacteria to cope with sudden nitrogen availability. Quantitative tracking of the dynamic intracellular metabolome and metabolic fluxes in response to the perturbation allowed us to identify active cycling between ornithine and arginine in the nondiazotrophic *Synechocystis* sp. PCC 6803 and diazotrophic *Cyanothece* sp. ATCC 51142. Then, through genetic and biochemical characterization, we identified an arginine dihydrolase, ArgZ, that catalyzes the conversion of arginine into ornithine and ammonia. Our results led to the discovery of an OAC and the identification of its function as nitrogen storage-and-remobilization machinery that is essential for cyanobacterial cells to adapt to environmental nitrogen oscillations.

Results

Arginine biosynthetic pathway responds to nitrate upshift. We grew a model cyanobacterium *Synechocystis* sp. PCC 6803 (hereafter denoted *Synechocystis*) in filter cultures[20] with nitrate as the nitrogen source (Fig. 1a). At a low initial concentration of nitrate (2 mM), the filter culture grew at an unlimited rate for 48 h to approximately 3×10^9 cells. Thereafter, the cell growth rate markedly decreased. In agreement with the culture being nitrogen limited, the cells became yellow-green, thus indicating the start of chlorosis. After the nitrogen-limited filter culture was transferred

[1]CAS-Key Laboratory of Synthetic Biology, CAS Center for Excellence in Molecular Plant Sciences, Shanghai Institute of Plant Physiology and Ecology, Chinese Academy of Sciences, Shanghai, China. [2]University of Chinese Academy of Sciences, Beijing, China. [3]State Key Laboratory of Bioreactor Engineering, East China University of Science and Technology, Shanghai, China. [4]State Key Lab of Genetic Engineering & Center for Synthetic Biology, Department of Microbiology and Microbial Engineering, School of Life Sciences, Fudan University, Shanghai, China. [5]Department of Microbiology and Li Ka Shing Institute of Health Sciences, Chinese University of Hong Kong, Prince of Wales Hospital, Shatin, Hong Kong SAR, China. *e-mail: chenyang@sibs.ac.cn

to medium containing 18 mM nitrate, cell growth was immediately and fully restored, exhibiting a rate of approximately 0.5 h^{-1}, a value almost identical to the growth rate of the culture with 18 mM initial nitrate (Fig. 1a).

To obtain a global view of the metabolic response to nitrate upshift, we measured the metabolomic changes at various time points after transferring the nitrogen-limited filter culture to nitrate-replete medium. Intracellular metabolites were rapidly extracted and then analyzed by liquid chromatography (LC)–MS, which enabled quantification of 230 metabolites (Supplementary Fig. 1). We found that within 1 min after nitrate upshift, the intracellular concentration of α-ketoglutarate decreased by about 80% , whereas the glutamine concentration increased over 15-fold (Fig. 1b). This result was consistent with these two metabolites being the central players in nitrogen assimilation. Interestingly, among the metabolites most severely affected by nitrate upshift, we observed a considerable and rapid increase in the concentrations of arginine-biosynthetic-pathway intermediates including *N*-acetylornithine, ornithine, citrulline, and argininosuccinate (Fig. 1b). These metabolites increased 10- to 120-fold within 30 min of the perturbation, thus suggesting a rapid response of the arginine biosynthetic pathway to nitrate upshift. This result prompted us to perform a quantitative analysis of arginine biosynthesis in *Synechocystis* during rapid recovery from nitrogen starvation.

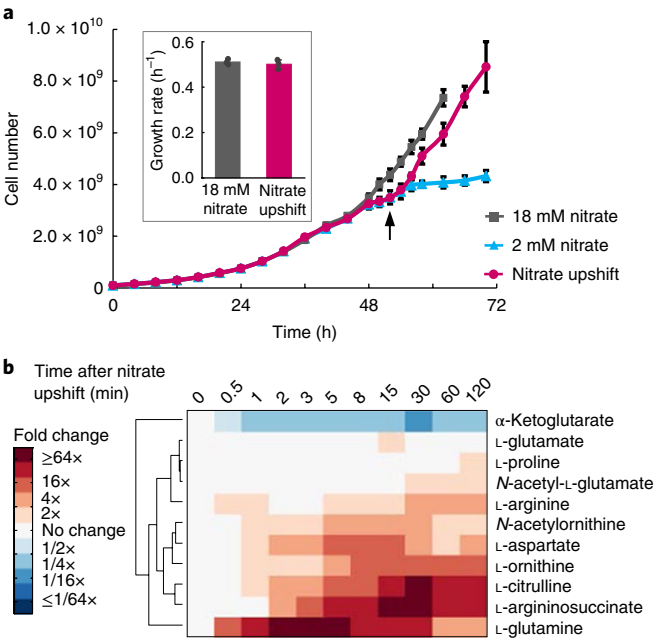

Fig. 1 | Cell growth and metabolomic response to nitrate upshift. a, Growth of *Synechocystis* in filter cultures. For nitrate upshift experiments, cells were grown on 2 mM nitrate for ~48 h and then switched (as indicated by the arrow) to medium containing 18 mM nitrate. Data shown are mean ± s.d. ($n = 3$ independent experiments). Inset, cell growth rate after nitrate upshift compared with that of the culture with 18 mM initial nitrate. Data shown are mean ± s.d. ($n = 3$ independent experiments). **b**, Metabolomic changes induced by nitrate upshift. Data are shown in heat-map format, with each row showing the time-dependent concentration change in an individual metabolite after the perturbation. Metabolite concentrations of two cell cultures were averaged and normalized to those of nitrogen-starved cells (time zero), and the resulting fold changes were $\log_2$ transformed. Complete data are shown in Supplementary Fig. 1.

Identification of cycling between ornithine and arginine. To quantify the flux through the arginine biosynthetic pathway in response to sudden nitrogen availability, we conducted dynamic ^{15}N and ^{13}C labeling experiments on filter cultures by using [^{15}N]nitrate or uniformly labeled (*U*) [*U*-^{13}C]glutamate as tracers. We transferred the nitrogen-limited cultures to nitrogen-replete medium containing [^{15}N]nitrate or [*U*-^{13}C]glutamate and then analyzed the dynamic labeling of individual metabolites through rapid and frequent sampling and LC–MS/MS measurements (Supplementary Fig. 2 and Supplementary Fig. 3). Arginine is synthesized from ornithine via ornithine transcarbamoylase (OTC), argininosuccinate synthase, and argininosuccinate lyase, with four nitrogen atoms derived from ornithine, glutamine, and aspartate (Fig. 2a). The dynamic labeling data of citrulline, glutamine, and ornithine allowed us to quantify the OTC flux (Fig. 2b). Then, by subtracting the accumulation rates of the citrulline and argininosuccinate pools, we determined the arginine synthetic flux through argininosuccinate lyase to be 0.28 nmol μL^{-1} min^{-1} (in which volume is the packed cell volume). Given that the measured nitrogen-assimilating flux through GS was 6.3 nmol μL^{-1} min^{-1}, a large fraction (~20%) of the total assimilated nitrogen was directed to the arginine biosynthetic pathway in cells exposed to a sudden nitrate upshift.

Arginine can be produced through both de novo synthesis and protein degradation. We found that the extent of arginine labeling was substantially lower than that of its precursor, argininosuccinate (Fig. 2b). The decrease in the labeled fraction was also observed for other amino acids, such as proline, because protein degradation feeds unlabeled nitrogen and carbon into free amino acids[25,26]. The resulting flux to arginine was determined to be 0.054 nmol μL^{-1} min^{-1} during cell recovery from nitrogen starvation (Fig. 2c). However, arginine is consumed for synthesis of cyanophycin in cyanobacteria, beyond its role as a precursor for synthesis of biomass components (protein) and polyamines. The fluxes of arginine to cyanophycin, biomass, and polyamines after nitrate upshift were measured to be 0.11, 0.081, and 0.0055 nmol μL^{-1} min^{-1}, respectively (Fig. 2c). Because the accumulation rate of the arginine pool is negligible relative to the arginine synthetic flux, the total consumption and production of arginine must be equal. However, we found that the total arginine influx exceeded the sum of its effluxes (Fig. 2c), thus suggesting the presence of an additional yet-uncharacterized arginine-consuming metabolic pathway.

Ornithine is synthesized from *N*-acetylglutamate (NAG) in the arginine biosynthetic pathway (Fig. 2a). We developed an ordinary differential equation (ODE) model to simulate the labeling kinetics of ornithine from the measured data for NAG. However, simulation with this model was inconsistent with the experimental data (Fig. 2d). We therefore augmented the model with other potential routes of ornithine synthesis. The model including ornithine formation from proline also did not match the experimental data. However, the model including ornithine synthesis from arginine well captured the experimentally determined labeling kinetics of ornithine (Fig. 2d). The flux of arginine to ornithine was found to be 0.14 nmol μL^{-1} min^{-1}, accounting for 42% of the total ornithine synthesis (Fig. 2e). Moreover, this arginine efflux allowed for the total consumption and production of arginine to be balanced. Thus, on the basis of the dynamic labeling experiments and quantitative flux analysis, we hypothesized that active cycling between ornithine and arginine occurred in *Synechocystis* exposed to nitrate upshift. We observed that this cyclic pathway was also probably present but at low activity in cells exponentially growing on replete nitrate (Supplementary Fig. 4a). Next, we sought to investigate whether ornithine is indeed synthesized from arginine by an unidentified enzyme in *Synechocystis*.

Deletion of the *argZ* gene results in arginine accumulation. To identify the enzyme catalyzing the conversion of arginine to ornithine, we deleted the genes *sll0228*, *sll1077*, and *sll1336* encoding putative arginine-degrading enzymes in *Synechocystis*

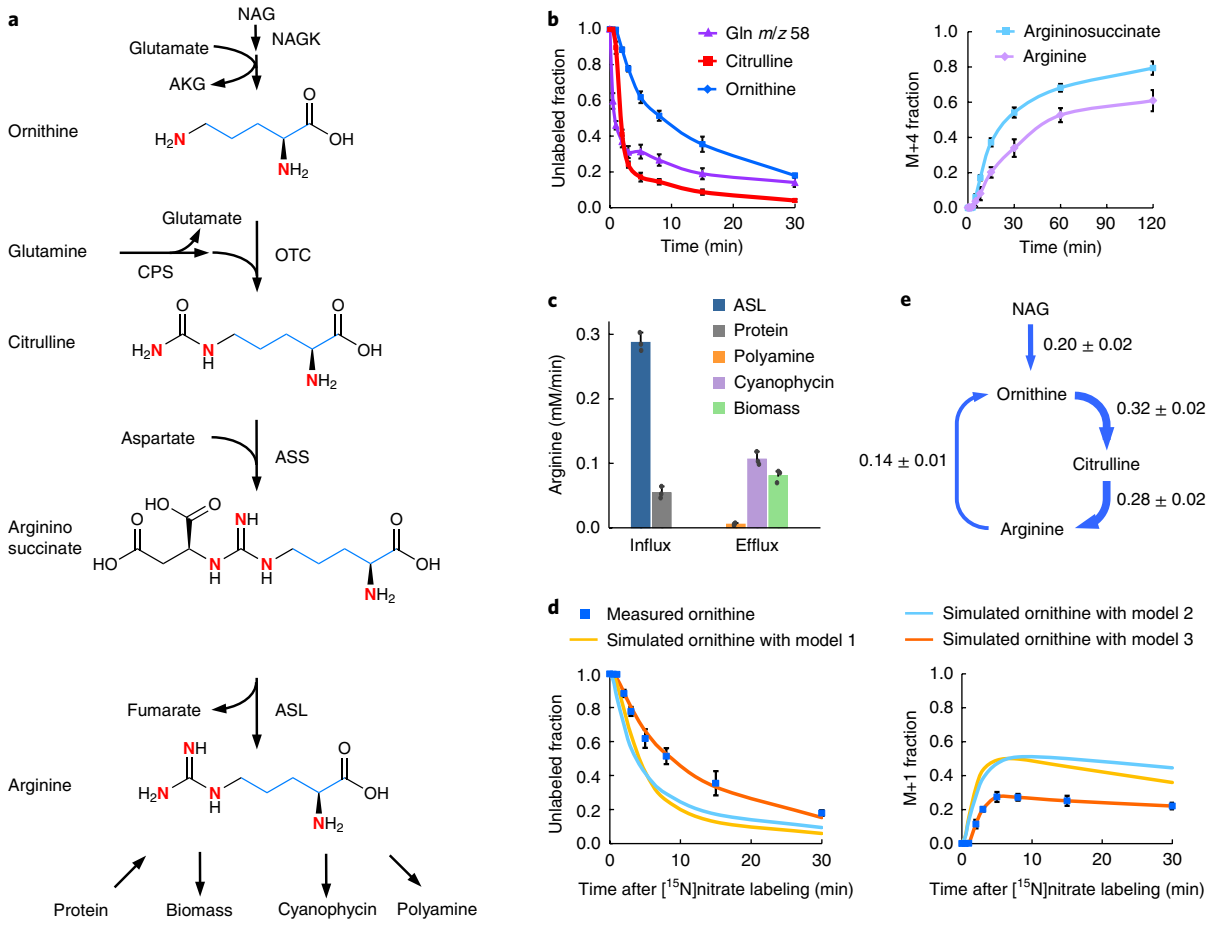

Fig. 2 | Identification of active cycling between ornithine and arginine. a, Schematic of [^{15}N]nitrate- or [*U*-^{13}C]glutamate-derived labeling through the arginine biosynthetic pathway. Labeled nitrogen and carbon are shown in red and blue, respectively. NAGK, NAG kinase; AKG, α-ketoglutarate; ASS, argininosuccinate synthase; ASL, argininosuccinate lyase. **b**, Kinetics of labeling of arginine-biosynthetic-pathway intermediates after switching nitrogen-starved cells to [^{15}N]nitrate medium. Data shown are mean ± s.d. ($n = 3$ independent experiments). Complete labeling data are shown in Supplementary Fig. 2 and Supplementary Fig. 3. **c**, Comparison of arginine production and consumption after nitrate upshift. Data shown are mean ± s.d. ($n = 3$ independent experiments). **d**, Comparison of measured and simulated labeling data for ornithine. Data shown are mean ± s.d. ($n = 3$ independent experiments). The yellow line shows the simulation with a model assuming that ornithine is generated entirely from NAG (model 1). The blue line shows simulation with a model including ornithine synthesis from proline (model 2). The orange line shows simulation with a model including ornithine formation from arginine (model 3). **e**, In vivo cyclic fluxes through ornithine and arginine in *Synechocystis* exposed to nitrate upshift. Data shown are median ± 95% confidence interval ($n = 3$ independent experiments) and are expressed in nmol per μL cell volume per min. Arrow sizes are scaled to the flux values.

(Supplementary Fig. 5). Sll0228 and Sll1077 are annotated as arginases, and the hypothetical protein Sll1336 has been proposed to be an arginine deiminase, on the basis of bioinformatics analysis[27]. We grew the gene-deletion mutants and wild-type strain on arginine as the nitrogen source and compared their intracellular metabolite concentrations. The *sll0228*- or *sll1077*-knockout mutants were able to grow on arginine and did not accumulate intracellular arginine (Fig. 3a,b), a result consistent with a previous finding that both genes may encode other ureohydrolases rather than arginases[28]. In contrast, deletion of *sll1336* abolished the growth of the resulting strain on arginine but did not affect its growth on nitrate (Fig. 3a). We observed that *sll1336* knockout led to accumulation of arginine and depletion of ornithine when the cells were switched to medium containing arginine (Fig. 3c). These results indicate that *sll1336* encodes a major arginine-degradation enzyme, and thus we propose to designate this gene *argZ*.

To test whether ArgZ functions in the cycling between ornithine and arginine, we investigated the effects of *argZ* deletion on metabolite concentrations and fluxes during nitrate upshift. We transferred the *argZ*-deletion mutant from nitrogen-limiting to nitrogen-replete medium and conducted [^{15}N]nitrate and [*U*-^{13}C]glutamate dynamic labeling experiments. The experimentally determined labeling kinetics of ornithine in the *argZ* mutant fit the model assuming that ornithine is generated entirely from NAG (Fig. 3d). This result suggests that the conversion of arginine to ornithine is blocked in the *argZ* mutant. Moreover, the *argZ* mutant, compared with the wild type, exhibited markedly higher levels of arginine and lower ornithine concentrations (Fig. 3e and Supplementary Fig. 4b). Therefore, these results suggest that ArgZ is required to convert arginine to ornithine in *Synechocystis*. In addition, we found that the fluxes through NAG kinase and OTC decreased by 35% and 65%, respectively, in the *argZ* mutant compared with the wild type during nitrate upshift, thus indicating that arginine biosynthesis was impaired in the mutant (Fig. 3f). This result may be explained by modulation of NAG kinase and CPS activities by arginine and ornithine, respectively[29,30] (Supplementary Fig. 6).

ArgZ converts arginine to ornithine and ammonia. The ArgZ protein exhibits ~10% sequence identity to amidinotransferase family proteins (Pfam PF02274) comprising glycine and lysine amidinotransferases and arginine deiminases (Supplementary Fig. 7a). ArgZ also contains a lysine–α-ketoglutarate reductase/

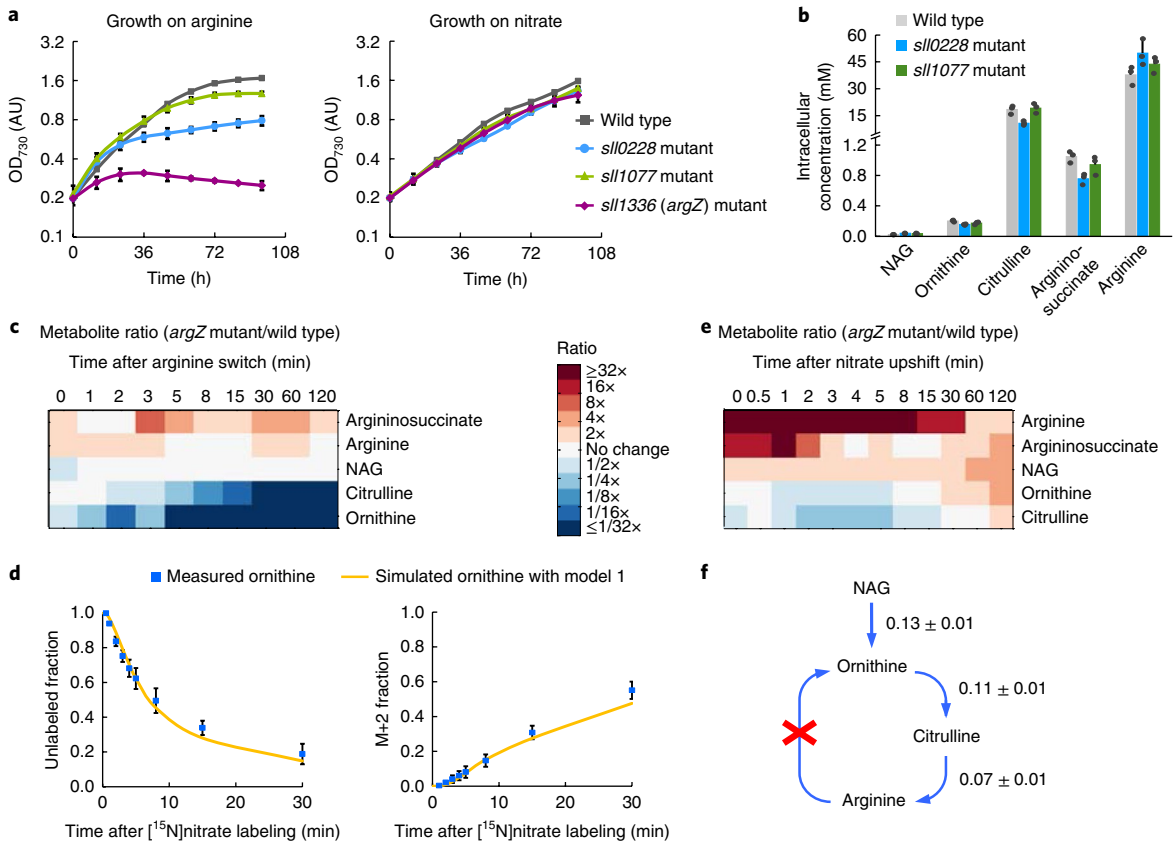

Fig. 3 | Deletion of *argZ* results in arginine accumulation. a, Effects of deletion of genes *sll0228*, *sll1077*, and *sll1336* (*argZ*) on *Synechocystis* cell growth on arginine or nitrate as the nitrogen source. OD_{730}, optical density at 730 nm. Data shown are mean ± s.d. ($n = 3$ independent experiments). **b**, Intracellular metabolite concentrations in wild type and *sll0228*- and *sll1077*-deleted mutants exponentially growing on arginine. Data shown are mean ± s.d. ($n = 3$ independent experiments). **c**, Ratio of metabolite concentrations in the *argZ* mutant versus wild type after arginine switch. The nitrate-grown filter culture was transferred to medium containing arginine as the nitrogen source. **d**, Comparison of measured and simulated labeling data for ornithine. Data shown are mean ± s.d. ($n = 3$ independent experiments). The yellow line shows the simulation with a model assuming that ornithine is generated entirely from NAG (model 1). **e**, Ratio of metabolite concentrations in the *argZ* mutant versus wild type after nitrate upshift. In **c** and **e**, data are means of three independent experiments, normalized to the values in the wild type, and $\log_2$ transformed. **f**, In vivo metabolic fluxes through ornithine and arginine in the *argZ*-mutant strain after nitrate upshift. The red X indicates blockade of the reaction. Data shown are median ± 95% confidence interval ($n = 3$ independent experiments) and are expressed in nmol per μL cell volume per min. Arrow sizes are scaled to the flux values.

saccharopine dehydrogenase conserved region of undefined function (Pfam PF04455). To confirm that ArgZ catalyzes the conversion of arginine to ornithine, we performed biochemical assays using purified recombinant ArgZ protein from *Synechocystis* (Supplementary Fig. 7b). Incubation of ArgZ with arginine led to the formation of ornithine, which was identified by HPLC and further validated by LC–MS (Fig. 4a,b). This result indicated that ArgZ is not an arginine deiminase catalyzing citrulline formation from arginine. Further analyses indicated that ArgZ is neither an amidinotransferase nor an arginase (Supplementary Fig. 7c,d). In fact, ammonia was detected in the reaction products through both HPLC and an enzymatic assay (Fig. 4a,c). We then performed HPLC analysis of the assay mixture to quantify the ArgZ-catalyzed formation of ornithine and ammonia from arginine. The molar amounts of arginine consumption and ornithine formation were almost identical, and the molar ratio of ammonia to ornithine formation was approximately 2.0 (Fig. 4d). In addition, formation of carbon dioxide by the ArgZ reaction was detected by gas chromatography. Thus, we propose that ArgZ converts arginine to ornithine with the release of ammonia and carbon dioxide (Supplementary Fig. 7e).

To our knowledge, ArgZ is the first arginine dihydrolase identified. Unlike arginases and arginine deiminases, arginine dihydrolase does not require Mg^{2+} or Mn^{2+} for optimal activity (Supplementary Fig. 7f). It is highly specific to arginine and is incapable of hydrolyzing citrulline, dimethylarginine, and other amino acids (Fig. 4c and Supplementary Fig. 7g). Kinetic characterization of ArgZ toward arginine showed a k_{cat} of 6.4 s^{-1} and K_m of 0.51 mM, which is within the physiological concentration range of arginine in *Synechocystis* (Supplementary Fig. 7h). In addition, we found that the N-terminal domain of ArgZ is responsible for catalysis (Supplementary Fig. 7i,j). Further studies are needed to provide insights into the catalytic mechanism of arginine dihydrolase.

OAC is required for cellular adaptation to nitrogen oscillation. On the basis of the in vivo and in vitro experimental results described above, an OAC was identified in *Synechocystis*. This cycle directs assimilated nitrogen in the form of glutamine and aspartate to synthesis of the nitrogen-rich arginine, which can further generate the nitrogen reservoir cyanophycin (Fig. 5a). To test whether the OAC is coupled with the nitrogen assimilation pathway, we compared the GS–GOGAT cycle flux between the wild type and *argZ* mutant during nitrate upshift, in a [^{15}N]nitrate dynamic labeling experiment. The fluxes through GS and GOGAT in the *argZ* mutant decreased by approximately 35%, thus indicating that disruption of OAC hampers the rapid assimilation of nitrogen during cell recovery from nitrogen starvation (Supplementary

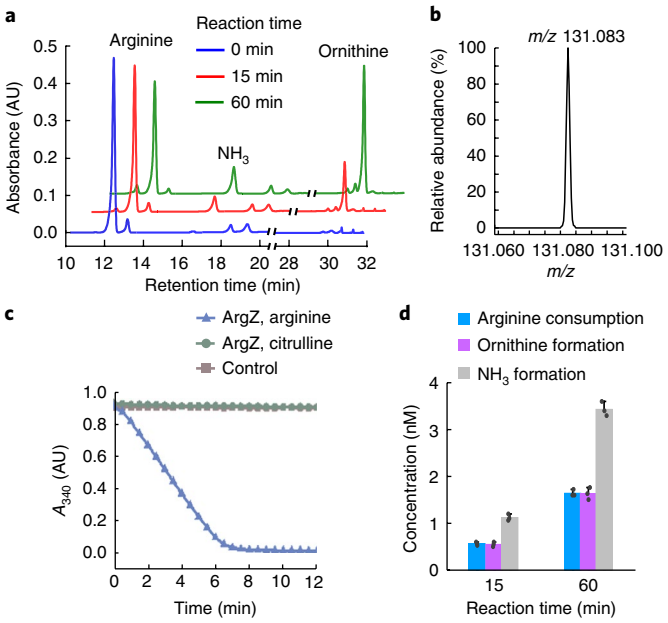

Fig. 4 | Characterization of the arginine dihydrolase ArgZ. a, HPLC analysis of reaction products. The reaction mixture containing arginine was analyzed before (0 min) and 15 min and 60 min after addition of purified ArgZ. **b**, LC–MS analysis of ornithine produced by the enzymatic reaction. **c**, Assay of ammonia-forming activity of ArgZ determined through coupling to the oxidation of NADH to NAD^+ via glutamate dehydrogenase and monitoring the absorbance at 340 nm. No activity was detected in control experiments using boiled enzyme or using citrulline to replace arginine in the assay mixture. Data in **a**–**c** are representative of $n = 3$ independent experiments that yielded identical results. **d**, Determination of ArgZ-catalyzed formation of ornithine and ammonia from arginine, through HPLC analysis of the assay mixture. Data shown are mean ± s.d. ($n = 3$ independent experiments).

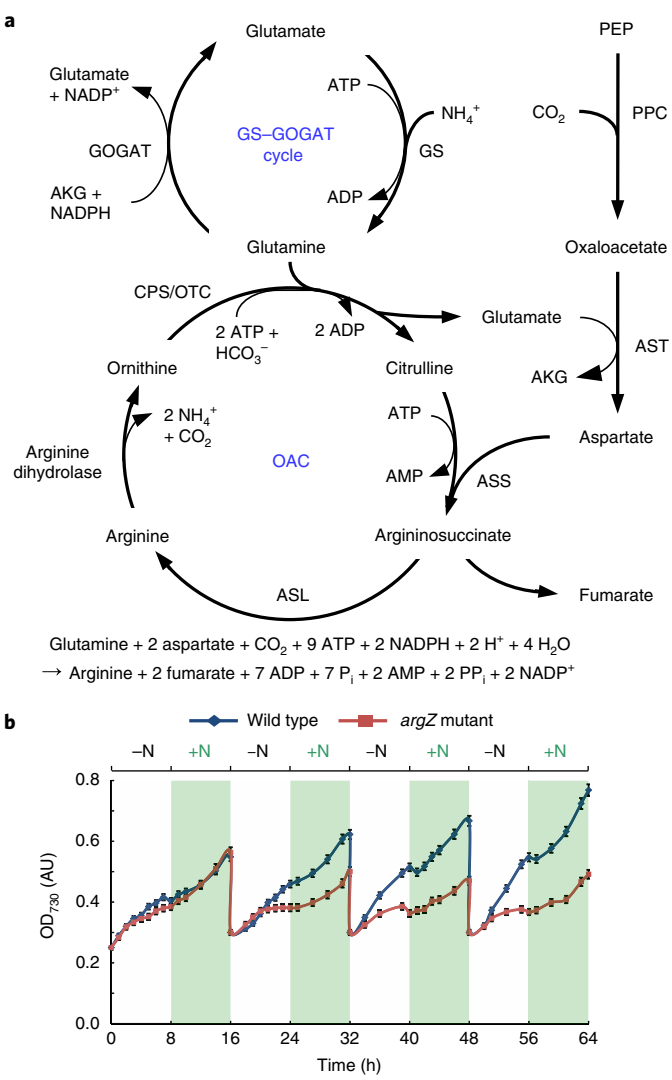

Fig. 5 | OAC couples with the GS–GOGAT cycle and PPC reaction. a, Schematic showing the direct connections among the OAC, the GS–GOGAT cycle, and the PPC reaction. Bottom, overall equation of the OAC. AST, aspartate aminotransferase; P_i, inorganic phosphate. **b**, Growth of *Synechocystis* wild type and *argZ* mutant under nitrogen-oscillation conditions. Cells were grown on nitrogen-free (–N) medium and nitrogen-replete (+N) medium supplied every 8 h. Data shown are mean ± s.d. ($n = 3$ independent experiments).

Fig. 6). This result is probably due to the higher aspartate levels in the *argZ* mutant than the wild type (Supplementary Fig. 6), which can inhibit GS and GOGAT activity[31,32]. In addition, an association between OAC and phosphoenolpyruvate (PEP) carboxylase (PPC) was apparent. We determined the CO_2-fixation fluxes in a [^{13}C]bicarbonate dynamic labeling experiment. The flux through PPC was 2.8 nmol μL^{-1} min^{-1}, which contributed 17% of overall CO_2 fixation in the wild type after nitrate upshift (Supplementary Fig. 6). We found that the PPC flux decreased by 65% in the *argZ* mutant. Together, these results illustrate important connections among the OAC, the nitrogen-assimilating GS–GOGAT cycle, and the CO_2-fixing PPC reaction.

To test whether the OAC might be useful for rapidly consuming arginine and cyanophycin to provide nitrogen under nitrogen starvation, we transferred the wild type and *argZ* mutant from nitrogen-limiting medium to nitrogen-replete medium containing [^{15}N]nitrate, then removed the nitrogen source or switched to medium containing [*U*-^{13}C, *U*-^{15}N]arginine (Supplementary Fig. 8). On the basis of the labeling kinetics of OAC-related metabolites, we observed rapid synthesis of ornithine from consumption of internal arginine and cyanophycin in the wild type after nitrogen deprivation. The ^{15}N label from arginine was rapidly incorporated into ornithine and ammonia in the wild type. Ammonia was immediately assimilated by GS to form glutamine, and ornithine was used to generate proline and glutamate (Supplementary Fig. 8). In contrast, the ^{15}N label from arginine was not detected in ornithine and glutamine in the *argZ* mutant. Thus, the OAC allows for rapid recycling of nitrogen stored in arginine and cyanophycin under nitrogen starvation.

To determine the physiological importance of the OAC, we studied the effect of disruption of OAC on *Synechocystis* cell growth during repeated cycles of nitrogen deprivation followed by replenishment treatments (Fig. 5b). Compared with the wild type, the *argZ* mutant showed lower growth rates on oscillating nitrate, particularly after the second removal of nitrate from the medium (Fig. 5b and Supplementary Fig. 9a,b). The phycocyanin content in the *argZ* mutant was lower than that in the wild type (Supplementary Fig. 9c,d). This result indicates that because the *argZ* mutant is unable to consume arginine and cyanophycin under nitrogen deprivation, it must degrade its phycobilisome antennae to provide nitrogen for cellular functions. Thus, the OAC enables cyanobacterial cells to adapt to varying nitrogen availability, including supporting normal growth under nitrogen deprivation and rapid growth resumption after a nitrogen source becomes available.

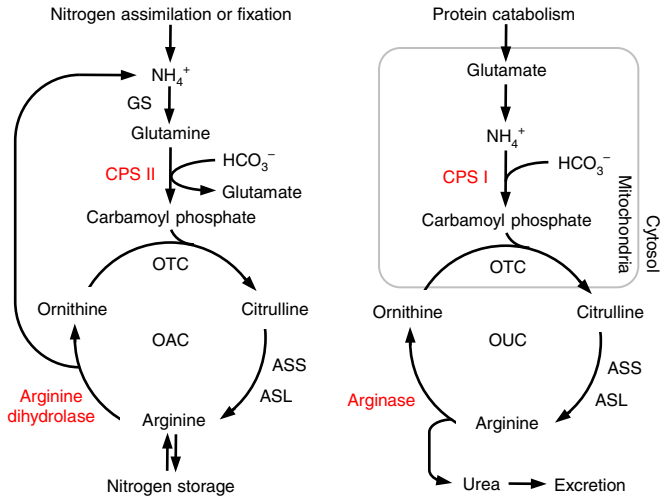

Fig. 6 | Comparison between the OAC and the OUC. Left, OAC; right, OUC. The different metabolic reactions of the two ornithine cycles are shown in red.

OAC is prevalent in cyanobacteria. The arginine dihydrolase is widely present among cyanobacteria exhibiting diverse morphological and physiological attributes. Notably, highly conserved homologs of arginine dihydrolase (>62% sequence identity) were identified in most diazotrophic cyanobacteria (Supplementary Fig. 10a), including the filamentous *Trichodesmium*, heterocyst-forming cyanobacteria such as *Anabaena*, and unicellular *Crocosphaera* and *Cyanothece*, which comprise the major groups of oceanic N_2-fixing cyanobacteria[33,34]. Because the ability to synthesize arginine from ornithine is found in virtually all organisms[1], the OAC may occur in these diazotrophic cyanobacteria. To test this possibility, we conducted dynamic labeling experiments on *Cyanothece* sp. ATCC 51142 (hereafter denoted *Cyanothece* 51142). This strain fixes nitrogen and accumulates cyanophycin granules during the night, whereas during the day, photosynthesis is performed, and cyanophycin is consumed as the major nitrogen source[12,35]. We switched cells from light to dark conditions and used [^{15}N]nitrate as a tracer to monitor the dynamic responses of the cellular metabolism. We observed highly similar patterns in the labeling kinetics of OAC intermediates between *Cyanothece* 51142 switched to dark conditions and *Synechocystis* exposed to nitrate upshift (Supplementary Fig. 10b–d), thus indicating that the OAC is active in *Cyanothece* 51142 under nitrogen-fixation conditions. *Cyanothece* cells probably use the OAC for storing and redistributing fixed nitrogen within cyanophycin.

Discussion

Living organisms have evolved mechanisms for adjusting their metabolism to adapt to environmental stress and nutrient availability. The OUC, which has evolved in terrestrial animals for disposal of excess nitrogen derived from protein in the diet, is generally accepted to be absent in bacteria and plants[4,5] (Fig. 6). In this study, by combining use of dynamic ^{15}N and ^{13}C tracers, metabolomics, and mathematical modeling, we discovered another ornithine cycle, OAC, in cyanobacteria, which starts with carbamoyl phosphate synthesis by the bacterial- and plant-type glutamine-dependent enzyme. Through genetic and biochemical characterization, we found that the last step of OAC is a novel reaction that converts arginine to ornithine and ammonia (Fig. 6). A mutant deficient in this enzyme showed disruption of the OAC and severe impairments in cell growth when nitrogen availability oscillated. We demonstrated that the OAC allows for mobilization of nitrogen reserves, priming the metabolism for a rapid response to nitrogen starvation. Moreover, the OAC is linked directly to the GS–GOGAT cycle and enables nitrogen assimilation and storage at a high rate after a nitrogen source becomes available. Thus, the OAC serves as a conduit in the nitrogen storage-and-remobilization machinery and confers cyanobacterial metabolism with substantial adaptability and robustness to environmental nitrogen fluctuations. Cyanobacteria may also use the OAC for storing and reallocating nitrogen within cyanophycin in response to changing light conditions or availability of other essential nutrients such as sulfur and phosphorus[10,36].

The OUC was long assumed to have originated in metazoans[1,37], although a recent report of its presence in diatoms suggests a much earlier origin for this pathway[3]. Our study indicates that the OAC might be a more ancient pathway than the OUC, because cyanobacteria have been widely distributed on the Earth since the Proterozoic Era (~2.3 billion years ago)[38]. Similarly to the OUC, the OAC may have also evolved from a previously existing arginine biosynthetic pathway[37]. Cyanobacteria appear to have evolved the OAC as an adaptation to many habitats, in which they are exposed to periodic nitrogen deficiency[39,40]. These findings raise the possibility that various types of ornithine cycle might have evolved in different organisms and prompt the intriguing question of whether an ornithine cycle might occur in other organisms with CPS type II, such as plants. For plants, similarly to cyanobacteria, nitrogen is often a limiting nutrient in the habitat, and arginine is a major storage form of organic nitrogen in plants[5]. The approaches described here could be appropriately adapted to test the possibility of metabolic cycling between ornithine and arginine in plants.

The OAC is widely distributed in cyanobacteria, particularly in marine N_2-fixing cyanobacteria. We presented evidence of an active OAC in the unicellular *Cyanothece* 51142, in which the OAC is used for storing and redistributing the fixed nitrogen within cyanophycin. Further studies are required to validate whether OAC has the same function in the filamentous *Trichodesmium* and heterocyst-forming species, which also utilize cyanophycin as a dynamic reservoir of fixed nitrogen[11,13]. Cyanobacteria possessing the OAC, whose lifestyles may be either free living or symbiotic with diatoms, are widely distributed through the warm oligotrophic ocean and play a crucial role in marine nitrogen fixation[33,34]. The integration of the OAC with N_2 fixation may have contributed to the success of these diazotrophs in the open ocean.

Methods

Methods, including statements of data availability and any associated accession codes and references, are available at https://doi.org/10.1038/s41589-018-0038-z.

Received: 25 September 2017; Accepted: 23 February 2018;
Published online: 9 April 2018

References

1. Jenkinson, C. P., Grody, W. W. & Cederbaum, S. D. Comparative properties of arginases. *Comp. Biochem. Physiol. B Biochem. Mol. Biol.* **114**, 107–132 (1996).
2. Mommsen, T. P. & Walsh, P. J. Evolution of urea synthesis in vertebrates: the piscine connection. *Science* **243**, 72–75 (1989).
3. Allen, A. E. et al. Evolution and metabolic significance of the urea cycle in photosynthetic diatoms. *Nature* **473**, 203–207 (2011).
4. Cunin, R., Glansdorff, N., Piérard, A. & Stalon, V. Biosynthesis and metabolism of arginine in bacteria. *Microbiol. Rev.* **50**, 314–352 (1986).
5. Winter, G., Todd, C. D., Trovato, M., Forlani, G. & Funck, D. Physiological implications of arginine metabolism in plants. *Front. Plant Sci.* **6**, 534 (2015).
6. Johnson, Z. I. et al. Niche partitioning among *Prochlorococcus* ecotypes along ocean-scale environmental gradients. *Science* **311**, 1737–1740 (2006).
7. Bergman, B., Sandh, G., Lin, S., Larsson, J. & Carpenter, E. J. *Trichodesmium*: a widespread marine cyanobacterium with unusual nitrogen fixation properties. *FEMS Microbiol. Rev.* **37**, 286–302 (2013).
8. Flores, E. & Herrero, A. Nitrogen assimilation and nitrogen control in cyanobacteria. *Biochem. Soc. Trans.* **33**, 164–167 (2005).

9. Schwarz, R. & Forchhammer, K. Acclimation of unicellular cyanobacteria to macronutrient deficiency: emergence of a complex network of cellular responses. *Microbiology* **151**, 2503–2514 (2005).
10. Allen, M. M. Inclusions: cyanophycin. *Methods Enzymol.* **167**, 207–213 (1988).
11. Burnat, M., Herrero, A. & Flores, E. Compartmentalized cyanophycin metabolism in the diazotrophic filaments of a heterocyst-forming cyanobacterium. *Proc. Natl Acad. Sci. USA* **111**, 3823–3828 (2014).
12. Li, H., Sherman, D. M., Bao, S. & Sherman, L. A. Pattern of cyanophycin accumulation in nitrogen-fixing and non-nitrogen-fixing cyanobacteria. *Arch. Microbiol.* **176**, 9–18 (2001).
13. Finzi-Hart, J. A. et al. Fixation and fate of C and N in the cyanobacterium *Trichodesmium* using nanometer-scale secondary ion mass spectrometry. *Proc. Natl Acad. Sci. USA* **106**, 6345–6350 (2009).
14. Wegener, K. M. et al. Global proteomics reveal an atypical strategy for carbon/nitrogen assimilation by a cyanobacterium under diverse environmental perturbations. *Mol. Cell. Proteomics* **9**, 2678–2689 (2010).
15. Osanai, T. et al. Capillary electrophoresis-mass spectrometry reveals the distribution of carbon metabolites during nitrogen starvation in *Synechocystis* sp. PCC 6803. *Environ. Microbiol.* **16**, 512–524 (2014).
16. Klotz, A. et al. Awakening of a dormant cyanobacterium from nitrogen chlorosis reveals a genetically determined program. *Curr. Biol.* **26**, 2862–2872 (2016).
17. Simons, M. et al. Nitrogen-use efficiency in maize (*Zea mays* L.): from 'omics' studies to metabolic modelling. *J. Exp. Bot.* **65**, 5657–5671 (2014).
18. Masakapalli, S. K., Kruger, N. J. & Ratcliffe, R. G. The metabolic flux phenotype of heterotrophic *Arabidopsis* cells reveals a complex response to changes in nitrogen supply. *Plant J.* **74**, 569–582 (2013).
19. Junker, B. H., Lonien, J., Heady, L. E., Rogers, A. & Schwender, J. Parallel determination of enzyme activities and in vivo fluxes in *Brassica napus* embryos grown on organic or inorganic nitrogen source. *Phytochemistry* **68**, 2232–2242 (2007).
20. Yuan, J., Bennett, B. D. & Rabinowitz, J. D. Kinetic flux profiling for quantitation of cellular metabolic fluxes. *Nat. Protoc.* **3**, 1328–1340 (2008).
21. van Heerden, J. H. et al. Lost in transition: start-up of glycolysis yields subpopulations of nongrowing cells. *Science* **343**, 1245114 (2014).
22. Buescher, J. M. et al. Global network reorganization during dynamic adaptations of *Bacillus subtilis* metabolism. *Science* **335**, 1099–1103 (2012).
23. Link, H., Kochanowski, K. & Sauer, U. Systematic identification of allosteric protein-metabolite interactions that control enzyme activity in vivo. *Nat. Biotechnol.* **31**, 357–361 (2013).
24. Xu, Y. F., Amador-Noguez, D., Reaves, M. L., Feng, X. J. & Rabinowitz, J. D. Ultrasensitive regulation of anapleurosis via allosteric activation of PEP carboxylase. *Nat. Chem. Biol.* **8**, 562–568 (2012).
25. Yuan, J. & Rabinowitz, J. D. Differentiating metabolites formed from de novo synthesis versus macromolecule decomposition. *J. Am. Chem. Soc.* **129**, 9294–9295 (2007).
26. Ishihara, H., Obata, T., Sulpice, R., Fernie, A. R. & Stitt, M. Quantifying protein synthesis and degradation in *Arabidopsis* by dynamic $^{13}CO_2$ labeling and analysis of enrichment in individual amino acids in their free pools and in protein. *Plant Physiol.* **168**, 74–93 (2015).
27. Schriek, S., Rückert, C., Staiger, D., Pistorius, E. K. & Michel, K. P. Bioinformatic evaluation of l-arginine catabolic pathways in 24 cyanobacteria and transcriptional analysis of genes encoding enzymes of l-arginine catabolism in the cyanobacterium *Synechocystis* sp. PCC 6803. *BMC Genomics* **8**, 437 (2007).
28. Quintero, M. J., Muro-Pastor, A. M., Herrero, A. & Flores, E. Arginine catabolism in the cyanobacterium *Synechocystis* sp. strain PCC 6803 involves the urea cycle and arginase pathway. *J. Bacteriol.* **182**, 1008–1015 (2000).
29. Delannay, S. et al. Serine 948 and threonine 1042 are crucial residues for allosteric regulation of *Escherichia coli* carbamoylphosphate synthetase and illustrate coupling effects of activation and inhibition pathways. *J. Mol. Biol.* **286**, 1217–1228 (1999).
30. Maheswaran, M., Urbanke, C. & Forchhammer, K. Complex formation and catalytic activation by the PII signaling protein of N-acetyl-l-glutamate kinase from *Synechococcus elongatus* strain PCC 7942. *J. Biol. Chem.* **279**, 55202–55210 (2004).
31. Orr, J. & Haselkorn, R. Kinetic and inhibition studies of glutamine synthetase from the cyanobacterium *Anabaena* 7120. *J. Biol. Chem.* **256**, 13099–13104 (1981).
32. Miller, R. E. & Stadtman, E. R. Glutamate synthase from *Escherichia coli*: an iron-sulfide flavoprotein. *J. Biol. Chem.* **247**, 7407–7419 (1972).
33. Zehr, J. P. Nitrogen fixation by marine cyanobacteria. *Trends Microbiol.* **19**, 162–173 (2011).
34. Sohm, J. A., Webb, E. A. & Capone, D. G. Emerging patterns of marine nitrogen fixation. *Nat. Rev. Microbiol.* **9**, 499–508 (2011).
35. Stöckel, J. et al. Global transcriptomic analysis of *Cyanothece* 51142 reveals robust diurnal oscillation of central metabolic processes. *Proc. Natl Acad. Sci. USA* **105**, 6156–6161 (2008).
36. Allen, M. M., Hutchison, F. & Weathers, P. J. Cyanophycin granule polypeptide formation and degradation in the cyanobacterium *Aphanocapsa* 6308. *J. Bacteriol.* **141**, 687–693 (1980).
37. Takiguchi, M., Matsubasa, T., Amaya, Y. & Mori, M. Evolutionary aspects of urea cycle enzyme genes. *BioEssays* **10**, 163–166 (1989).
38. Hamilton, T. L., Bryant, D. A. & Macalady, J. L. The role of biology in planetary evolution: cyanobacterial primary production in low-oxygen Proterozoic oceans. *Environ. Microbiol.* **18**, 325–340 (2016).
39. Canfield, D. E., Glazer, A. N. & Falkowski, P. G. The evolution and future of Earth's nitrogen cycle. *Science* **330**, 192–196 (2010).
40. Vitousek, P. M. & Howarth, R. W. Nitrogen limitation on land and in the sea: how can it occur. *Biogeochemistry* **13**, 87–115 (1991).

Acknowledgements

The authors thank Y. Shan for technical assistance on hybrid quadrupole-orbitrap MS and J. Zhao for helpful discussions. This work was funded for C.Y. by the National Natural Science Foundation of China (31630003 and 31470168), the National Key R&D Program of China (2016YFC1303303), and the Chinese Academy of Sciences (XDPB0400).

Author contributions

H.Z. performed most experiments and wrote the manuscript. Y.L. conducted biochemical assays. X.N. performed bioinformatics. L.L. contributed LC–MS analysis. Q.H. contributed mathematical modeling. G.-P.Z. contributed experimental design and discussion. C.Y. designed experiments, analyzed data, and wrote the manuscript.

Competing interests

The authors declare no competing interests.

Additional information

Supplementary information is available for this paper at https://doi.org/10.1038/s41589-018-0038-z.

Reprints and permissions information is available at www.nature.com/reprints.

Correspondence and requests for materials should be addressed to C.Y.

Publisher's note: Springer Nature remains neutral with regard to jurisdictional claims in published maps and institutional affiliations.

Methods

Strains and culture conditions. *Synechocystis* sp. PCC 6803 was routinely grown at 30 °C in BG-11 medium[41] under continuous white light (50 µmol quanta m^{-2} s^{-1}). *Cyanothece* sp. ATCC 51142 was cultivated at 30 °C in modified ASP2 medium without nitrate[42] under 12-h light/12-h dark conditions. The filter cultures were prepared as described previously[43]. Briefly, *Synechocystis* cells were initially grown in shake flasks to an OD_{730} of ~0.2 (corresponding to ~2×10^7 cells mL^{-1}). Five-milliliter aliquots of the culture were then passed through nitrocellulose membrane filters (0.45-µm pore size; Millipore). The filters were placed on top of agarose plates loaded with BG-11 medium containing nitrate as the nitrogen source. The initial concentrations of $NaNO_3$ in the medium were 18 mM or 2 mM. Cell growth was determined by washing the filter thoroughly with 5 mL of water and measuring the OD_{730}. For nitrate upshift experiments, filter cultures were grown on agarose plates with modified BG-11 medium containing 2 mM $NaNO_3$. After ~48 h, when the cell number reached ~3×10^9, the culture became nitrogen limited and was transferred to BG-11 plates containing 18 mM $NaNO_3$. For arginine-switch experiments, cells exponentially growing on nitrate were rapidly washed and transferred to BG-11 plates containing 5 mM arginine as the nitrogen source. For nitrogen-oscillation experiments, cells exponentially growing in 250-mL shake flasks with 100 mL BG-11 medium supplied with CO_2-enriched air (3% (vol/vol)) were harvested, washed with nitrogen-free minimal medium ($BG\text{-}11_{N0}$), and resuspended in 100 mL $BG\text{-}11_{N0}$ medium to an OD_{730} of ~0.3. After 8 h of nitrogen deprivation, 20 mM $NaNO_3$ was added to the culture, and cells were grown for another 8 h. Then the cycle of 8-h nitrogen deprivation followed by 8-h nitrogen repletion was repeated several times.

Dynamic isotope labeling experiments. Dynamic isotope labeling experiments were performed with ^{15}N-labeled $NaNO_3$ ([^{15}N]nitrate), [*U*-^{13}C]glutamate, ^{13}C-labeled $NaHCO_3$ ([^{13}C]bicarbonate), and [*U*-^{13}C, *U*-^{15}N]arginine as tracers. Labeled compounds were ≥99% pure and were purchased from Cambridge Isotope Lab. The filter cultures were transferred to BG-11 plates containing 18 mM [^{15}N] nitrate, 24 mM [^{13}C]bicarbonate, 2.5 mM [*U*-^{13}C, *U*-^{15}N]arginine, or 5 mM of a mixture of 50% (wt/wt) [*U*-^{13}C]glutamate and 50% unlabeled glutamate.

Metabolite measurements. Metabolism was quenched, and metabolites were extracted by rapid transfer of the filters into −20 °C 40:40:20 acetonitrile/methanol/water with 0.1% formic acid[44]. After incubation at −20 °C for 20 min, the samples were centrifuged, and the supernatant was collected.

Cell extracts were analyzed by ultrahigh performance liquid chromatograph (Acquity, Waters) coupled to a Q Exactive hybrid quadrupole–orbitrap mass spectrometer (Thermo Fisher). The injection volume was 10 µL. Solvent A was 20 mM ammonium acetate adjusted to pH 9.0 with ammonium hydroxide, and solvent B was acetonitrile. Metabolites were separated with a Luna NH2 column (100 mm × 2 mm, 3 µm particle size, Phenomenex). The column was maintained at 15 °C with a solvent flow rate of 0.3 mL min^{-1}, and the gradient of B was as follows: 0 min, 85%; 10 min, 45%; 15 min, 2%; 18 min, 2%; 18.1 min, 85%; 24 min 85% B. The mass spectrometer with a heated electrospray ionization source was operated in positive and negative modes. The key parameters were as follows: ionization voltage, +3.8 kV/−3.0 kV; sheath gas pressure, 35 arbitrary units; auxiliary gas, 10 arbitrary units; auxiliary gas heater temperature, 350 °C; capillary temperature, 320 °C. The mass spectrometer was run in full scan mode at an *m*/*z* 70–1,000 scan range and 70,000 resolution. Data processing and ion annotation based on accurate mass were performed in Xcalibur 4.0 (Thermo Fisher) and Compound Discoverer 2.0 (Thermo Fisher). A subset of identified compounds was verified by mass and retention-time match to authenticated standards.

MS/MS spectra for arginine and glutamine were acquired on the same mass spectrometer operated in negative ionization mode. Precursor ions of the metabolites were targeted as $[M\text{-}H]^-$ with a window size of 2 *m*/*z*. Fragmentation of the precursor ion was performed by higher-energy collisional dissociation at 30-eV collision energy. Fragment-ion spectra were recorded with 17,500 resolution. Peaks of fragment ions were extracted and matched with compounds in the Metlin database[45].

Mutant construction. *Synechocystis* mutants with knockout of the genes *sll1336* (*argZ*), *sll0228*, and *sll1077* were constructed as described previously[46]. PCR analyses were performed to verify replacement of the coding regions of individual genes with the kanamycin-resistance cassette and segregation of the mutant strains.

Enzyme assays. To identify the arginine-degrading activity of ArgZ, in vitro assays were performed using *Synechocystis* ArgZ after histidine-tag purification. After incubation of the purified enzyme with 5 mM L-arginine, the reaction products were identified by HPLC as described previously[47]. Ornithine produced by the enzymatic reaction was further confirmed with LC–MS as described above. Ammonia generated from arginine degradation was also determined enzymatically through measurement of the decrease in NADH concentration at 340 nm by using glutamate dehydrogenase as a coupling enzyme[48]. Carbon dioxide formed from the enzymatic reaction was detected through gas chromatography after the addition of 6 M HCl to stimulate release (GC7900, Techcomp).

The arginine dihydrolase activity was determined by addition of 1.0 µg of the purified enzyme to 200 µL of 50 mM triethanolamine buffer, pH 8.0, containing 5 mM L-arginine, 5 mM α-ketoglutarate, 0.2 mM NADH, and 5 U glutamate dehydrogenase. The change in NADH absorbance was monitored at 340 nm with a Beckman DU-800 spectrophotometer. The activity of arginine dihydrolase was expressed in µmol substrate converted per mg enzyme per min. To test the effects of metal ions on this activity, $MnCl_2$, $CoCl_2$, $MgCl_2$, NaCl, $CaCl_2$, $FeCl_3$, $FeSO_4$, $ZnSO_4$, or $CuSO_4$ (1.0 mM each) was added to the assay mixture. To test substrate specificity, L-arginine was replaced by 5 mM of citrulline, dimethylarginine, or individual proteinogenic amino acids in the assay mixture. For determination of the apparent k_{cat} and K_m values, the L-arginine concentration was varied in the range of 0.1 to 10 mM. Kinetic data were analyzed in GraphPad Prism 5.0.

Quantification of metabolic fluxes. The LC–MS data were analyzed as described previously[20]. Briefly, mass isotopomer distributions (MIDs) of intact and fragmented metabolites were calculated from measured peak areas of the mass spectra and corrected for naturally occurring ^{13}C. Each metabolic node of fluxes was modeled with a small-scale ODE system to simulate the dynamic labeling patterns of metabolites from the labeling patterns of their precursors. Model construction depended on the mapping of nitrogen or carbon atoms between substrates and products of the biochemical reactions composing the metabolic node, which is described in the following sections. The model was then used to identify the set of parameters including the fluxes or flux ratio of interest, which was compatible with the measured labeling patterns of metabolites. Parameters were fitted by minimizing the weighted sum of squared residuals (χ^2) between measured and simulated labeling kinetics. All calculations were performed in Matlab 7.8.0 (Mathworks).

Arginine-biosynthetic-pathway flux. The absolute flux through the arginine biosynthetic pathway was quantified on the basis of citrulline labeling kinetics. Cells were switched to medium containing [^{15}N]nitrate, and the dynamic MIDs of citrulline (CIT) and ornithine (ORN) were measured. Carbamoyl phosphate could not be detected by LC–MS. Because the nitrogen atom of carbamoyl phosphate is directly derived from the amide nitrogen of glutamine, the MS/MS-measured MID of the fragment ion of glutamine (Gln58) was used. The metabolic pseudo–steady state (i.e., when the sums of fluxes leading into and out of a pathway intermediate pool are equal) is assumed. Thus the MID of citrulline changes with time as:

$$\begin{aligned}
\frac{d\mathrm{CIT}_{m+0}}{dt} &= \frac{1}{C_{\mathrm{CIT}}}(v_{\mathrm{OTC}}\mathrm{ORN}_{m+0}\mathrm{Gln58}_{m+0} - v_{\mathrm{OTC}}\mathrm{CIT}_{m+0})\\
\frac{d\mathrm{CIT}_{m+1}}{dt} &= \frac{1}{C_{\mathrm{CIT}}}(v_{\mathrm{OTC}}(\mathrm{ORN}_{m+1}\mathrm{Gln58}_{m+0} + \mathrm{ORN}_{m+0}\mathrm{Gln58}_{m+1})\\
&\quad - v_{\mathrm{OTC}}\mathrm{CIT}_{m+1})\\
\frac{d\mathrm{CIT}_{m+2}}{dt} &= \frac{1}{C_{\mathrm{CIT}}}(v_{\mathrm{OTC}}(\mathrm{ORN}_{m+2}\mathrm{Gln58}_{m+0} + \mathrm{ORN}_{m+1}\mathrm{Gln58}_{m+1})\\
&\quad - v_{\mathrm{OTC}}\mathrm{CIT}_{m+2})\\
\frac{d\mathrm{CIT}_{m+3}}{dt} &= \frac{1}{C_{\mathrm{CIT}}}(v_{\mathrm{OTC}}\mathrm{ORN}_{m+2}\mathrm{Gln58}_{m+1} - v_{\mathrm{OTC}}\mathrm{CIT}_{m+3})
\end{aligned} \quad (1)$$

where v_{OTC} is the flux through ornithine transcarboxylase of the arginine biosynthetic pathway, and C_{CIT} is the pool size of citrulline. Equation (1) was used to determine v_{OTC} by fitting the simulated to the measured time-dependent MID of citrulline. The determined flux through citrulline was much higher than the accumulation rate of the citrulline pool, thus supporting the metabolic pseudo–steady state assumption.

Ornithine from NAG versus arginine. To quantify the relative contribution of NAG versus arginine in the formation of ornithine, cells were switched to medium containing [^{15}N]nitrate or [*U*-^{13}C]glutamate, and the labeling kinetics of ornithine, NAG, glutamate, and arginine was measured. The ODEs describing the MID dynamics of ornithine in the ^{15}N and ^{13}C labeling experiments are given by equations (2) and (3), respectively:

$$\begin{aligned}
\frac{d\mathrm{ORN}_{m+0}}{dt} &= \frac{1}{C_{\mathrm{ORN}}}(v_{\mathrm{NAG}}\mathrm{NAG}_{m+0}\mathrm{Glu}_{m+0} + v_{\mathrm{ARG}}\mathrm{Arg131}_{m+0}\\
&\quad - (v_{\mathrm{NAG}} + v_{\mathrm{ARG}})\mathrm{ORN}_{m+0})\\
\frac{d\mathrm{ORN}_{m+1}}{dt} &= \frac{1}{C_{\mathrm{ORN}}}(v_{\mathrm{NAG}}(\mathrm{NAG}_{m+1}\mathrm{Glu}_{m+0} + \mathrm{NAG}_{m+0}\mathrm{Glu}_{m+1})\\
&\quad + v_{\mathrm{ARG}}\mathrm{Arg131}_{m+1} - (v_{\mathrm{NAG}} + v_{\mathrm{ARG}})\mathrm{ORN}_{m+1})\\
\frac{d\mathrm{ORN}_{m+2}}{dt} &= \frac{1}{C_{\mathrm{ORN}}}(v_{\mathrm{NAG}}\mathrm{NAG}_{m+1}\mathrm{Glu}_{m+1} + v_{\mathrm{ARG}}\mathrm{Arg131}_{m+2}\\
&\quad - (v_{\mathrm{NAG}} + v_{\mathrm{ARG}})\mathrm{ORN}_{m+2})
\end{aligned} \quad (2)$$

$$\frac{d\mathrm{ORN}_{m+0}}{dt} = \frac{1}{C_{\mathrm{ORN}}}(v_{\mathrm{NAG}}\mathrm{NAG}_{m+0} + v_{\mathrm{ARG}}\mathrm{Arg}_{m+0} - (v_{\mathrm{NAG}} + v_{\mathrm{ARG}})\mathrm{ORN}_{m+0})$$
$$\frac{d\mathrm{ORN}_{m+5}}{dt} = \frac{1}{C_{\mathrm{ORN}}}(v_{\mathrm{NAG}}\mathrm{NAG}_{m+5} + v_{\mathrm{ARG}}\mathrm{Arg}_{m+5} - (v_{\mathrm{NAG}} + v_{\mathrm{ARG}})\mathrm{ORN}_{m+5}) \quad (3)$$

where v_{NAG} is the flux of ornithine synthesis from NAG, v_{ARG} is the flux of ornithine synthesis from arginine, and C_{ORN} is the pool size of ornithine. Arg131 is the MS/MS-measured fragment ion of arginine. Equations (2) and (3) were used to determine the flux ratio $v_{\mathrm{NAG}}/(v_{\mathrm{NAG}} + v_{\mathrm{ARG}})$.These equations were also used to simulate the labeling kinetics of ornithine when the flux ratio $v_{\mathrm{NAG}}/(v_{\mathrm{NAG}} + v_{\mathrm{ARG}})$ was set to a fixed value.

Nitrogen-assimilation-pathway fluxes. The fluxes through GS and GOGAT were quantified on the basis of the labeling kinetics of glutamine and glutamate from the [^{15}N]nitrate labeling experiment. The balances of the mass distribution for glutamine and glutamate were as follows.

$$\frac{d\mathrm{Gln}_{m+0}}{dt} = \frac{1}{C_{\mathrm{Gln}}}(v_{\mathrm{GS}}\mathrm{Glu}_{m+0}(1-L_{\mathrm{NH3}}) - v_{\mathrm{GS}}\mathrm{Gln}_{m+0})$$
$$\frac{d\mathrm{Gln}_{m+1}}{dt} = \frac{1}{C_{\mathrm{Gln}}}(v_{\mathrm{GS}}(\mathrm{Glu}_{m+1}(1-L_{\mathrm{NH3}}) + \mathrm{Glu}_{m+0}L_{\mathrm{NH3}}) - v_{\mathrm{GS}}\mathrm{Gln}_{m+1})$$
$$\frac{d\mathrm{Gln}_{m+2}}{dt} = \frac{1}{C_{\mathrm{Gln}}}(v_{\mathrm{GS}}\mathrm{Glu}_{m+1}L_{\mathrm{NH3}} - v_{\mathrm{GS}}\mathrm{Gln}_{m+2}) \quad (4)$$

$$\frac{d\mathrm{Glu}_{m+0}}{dt} = \frac{1}{C_{\mathrm{Glu}}}(v_{\mathrm{GOGAT}}\mathrm{Gln}_{m+0} + 0.5v_{\mathrm{GOGAT}}\mathrm{Gln}_{m+1} - v_{\mathrm{GOGAT}}\mathrm{Glu}_{m+0})$$
$$\frac{d\mathrm{Glu}_{m+1}}{dt} = \frac{1}{C_{\mathrm{Glu}}}(0.5v_{\mathrm{GOGAT}}\mathrm{Gln}_{m+1} + v_{\mathrm{GOGAT}}\mathrm{Gln}_{m+2} - v_{\mathrm{GOGAT}}\mathrm{Glu}_{m+1}) \quad (5)$$

where v_{GS} is the GS flux, v_{GOGAT} is the GOGAT flux, C_{Gln} and C_{Glu} are the pool sizes of glutamine and glutamate, respectively, and L_{NH3} is the degree of ^{15}N labeling of ammonia.

CO_2-fixation-pathway fluxes. To quantify the CO_2-fixation fluxes through PEP carboxylase and ribulose 1,5-bisphosphate (RuBP) carboxylase/oxygenase (Rubisco) in the Calvin–Benson–Bassham cycle, cells were switched to medium containing [^{13}C]bicarbonate, and the dynamic labeling patterns of PEP, RuBP, and 3-phosphoglyceric acid (PGA) were measured. Because oxaloacetate could not be detected by LC–MS, owing to its lability, we used the labeling kinetics of aspartate, which is formed from oxaloacetate by transamination. Thus equation (6) was obtained:

$$\frac{d\mathrm{Asp}_{m+0}}{dt} = \frac{1}{C_{\mathrm{Asp}}}(v_{\mathrm{PPC}}\mathrm{PEP}_{m+0}(1-L_{\mathrm{CO2}}) - v_{\mathrm{PPC}}\mathrm{Asp}_{m+0})$$
$$\frac{d\mathrm{Asp}_{m+1}}{dt} = \frac{1}{C_{\mathrm{Asp}}}(v_{\mathrm{PPC}}(\mathrm{PEP}_{m+1}(1-L_{\mathrm{CO2}}) + \mathrm{PEP}_{m+0}L_{\mathrm{CO2}}) - v_{\mathrm{PPC}}\mathrm{Asp}_{m+1}) \quad (6)$$

where v_{PPC} is the flux through PEP carboxylase, C_{Asp} is the pool size of aspartate, and L_{CO2} is the degree of ^{13}C labeling of CO_2. Equation (6) was used to estimate v_{PPC} by least-squares fitting. Similarly, the flux through Rubisco was estimated with equation (7).

$$\frac{d\mathrm{PGA}_{m+0}}{dt} = \frac{1}{C_{\mathrm{PGA}}}(v_{\mathrm{Rubisco}}(\mathrm{RuBP}_{m+0}(1-L_{\mathrm{CO2}}) + 0.5\mathrm{RuBP}_{m+0}L_{\mathrm{CO2}} + 0.5\mathrm{RuBP}_{m+1}(1-L_{\mathrm{CO2}})) - v_{\mathrm{Rubisco}}\mathrm{PGA}_{m+0})$$
$$\frac{d\mathrm{PGA}_{m+1}}{dt} = \frac{1}{C_{\mathrm{PGA}}}(v_{\mathrm{Rubisco}}(0.5\mathrm{RuBP}_{m+0}L_{\mathrm{CO2}} + 0.5\mathrm{RuBP}_{m+1}(1-L_{\mathrm{CO2}}) + \mathrm{RuBP}_{m+1}L_{\mathrm{CO2}}) - v_{\mathrm{Rubisco}}\mathrm{PGA}_{m+1}) \quad (7)$$

where v_{Rubisco} is the flux through Rubisco, and C_{PGA} is the pool size of PGA.

Arginine effluxes to biomass, cyanophycin, and polyamines. The flux of arginine to cyanophycin was quantified from the experimentally measured accumulation rate of cyanophycin[47]. The arginine efflux to biomass was calculated on the basis of previously reported *Synechocystis* biomass composition[49] and experimentally determined cell growth rate. The flux of arginine to polyamines was determined on the basis of the labeling kinetics of agmatine from the [^{15}N]nitrate labeling experiment.

Statistics. Unless noted otherwise, data are presented as the mean ± s.d. of n independent experiments, and P values were calculated with two-tailed Student's t test. For fluxes, the best estimates were obtained by minimizing the deviation between experimental and simulated metabolite labeling kinetics, as described above. The flux 95% confidence interval was determined on the basis of Monte Carlo simulations by repeatedly resampling the experimental data from a normal distribution (with s.d. equivalent to the experimentally determined s.d.) and calculating the fluxes that minimized the deviation between this resampled experimental data and simulated metabolite labeling data[50]. Statistics were generated in Matlab or Microsoft Excel.

Reporting Summary. Further information on experimental design is available in the Nature Research Reporting Summary linked to this article.

Data availability. All the data generated or analyzed during this study are available within the manuscript and its Supplementary Information files.

References

41. Rippka, R., Deruelles, J., Waterbury, J. B., Herdman, M. & Stanier, R. Y. Generic assignments, strain histories and properties of pure cultures of cyanobacteria. *Microbiology* **111**, 1–61 (1979).
42. Reddy, K. J., Haskell, J. B., Sherman, D. M. & Sherman, L. A. Unicellular, aerobic nitrogen-fixing cyanobacteria of the genus *Cyanothece*. *J. Bacteriol.* **175**, 1284–1292 (1993).
43. Gao, X. et al. Engineering the methylerythritol phosphate pathway in cyanobacteria for photosynthetic isoprene production from CO_2. *Energy Environ. Sci.* **9**, 1400–1411 (2016).
44. Rabinowitz, J. D. & Kimball, E. Acidic acetonitrile for cellular metabolome extraction from *Escherichia coli*. *Anal. Chem.* **79**, 6167–6173 (2007).
45. Tautenhahn, R. et al. An accelerated workflow for untargeted metabolomics using the METLIN database. *Nat. Biotechnol.* **30**, 826–828 (2012).
46. Golden, S. S., Brusslan, J. & Haselkorn, R. Genetic engineering of the cyanobacterial chromosome. *Methods Enzymol* **153**, 215–231 (1987).
47. Liu, D. & Yang, C. The nitrogen-regulated response regulator NrrA controls cyanophycin synthesis and glycogen catabolism in the cyanobacterium *Synechocystis* sp. PCC 6803. *J. Biol. Chem.* **289**, 2055–2071 (2014).
48. Tocilj, A. et al. Crystal structure of N-succinylarginine dihydrolase AstB, bound to substrate and product, an enzyme from the arginine catabolic pathway of *Escherichia coli*. *J. Biol. Chem.* **280**, 15800–15808 (2005).
49. Young, J. D., Shastri, A. A., Stephanopoulos, G. & Morgan, J. A. Mapping photoautotrophic metabolism with isotopically nonstationary ^{13}C flux analysis. *Metab. Eng.* **13**, 656–665 (2011).
50. Hörl, M., Schnidder, J., Sauer, U. & Zamboni, N. Non-stationary ^{13}C-metabolic flux ratio analysis. *Biotechnol. Bioeng.* **110**, 3164–3176 (2013).